Macroscopic chemical to electrical signal converter in microbial communities

M. García-Navarrete[1,†], Merisa Avdovic[1,†], S. Pérez García[1,†], D. Ruiz Sanchis[1], K. Wabnik[1,*]

[1] Centro de Biotecnologıa y Genomica de Plantas (Universidad Politecnica de Madrid – Instituto Nacional de Investigacion y Tecnologıa Agraria y Alimentaria), Autopista M-40, Km 38 – 28223 Pozuelo de Alarcon, Spain

†Contributed equally

*Corresponding author. Email: k.wabnik@upm.es

Summary

Excitable nerve cells convert electrical signals into chemical outputs to facilitate the active transport of information across the nervous system. We engineered unicellular microbe *S. cerevisiae* to directly read and convert local chemical concentrations into a dynamic electrical field that is uniformly distributed across fungi populations. The chemically-excitable dual-feedback gene circuit precisely tunes the expression of active potassium channels, coordinating cyclic firing of the plasma membrane potential (PMP). Our findings provide mechanistic insights into how cells transform local chemical environments into electrical signals to guide coordinated behavior at the macroscopic scale.

Communication through electrical signals provides an effective mechanism for the rapid delivery of information across noisy cells and tissues. Prominent examples of this phenomenon across kingdoms include excitable neuronal circuits[1], plant defense signaling[2], and metabolic coordination of biofilm growth[3]. These seemingly different forms of electrical signaling involve common mediators, the voltage-gated potassium channels[4]. Outward-rectifying potassium channels release potassium ions from the intracellular reservoir to the extracellular space, thereby allowing for potassium exchange between neighboring cells[5]. A rapid gating of ion channels at the subcellular level maintains the balance in the plasma membrane potential (PMP), which in turn provides power reservoir and electrical communication routes[6]. Typically, rapid electrical signals generated by cells such as neurons are processed into slower biochemical outcomes but rarely vice versa. How do local chemical signals are effectively converted by cells into robust electrical fields capable of coupling entire populations remains largely unexplored.

To address this intriguing dilemma, we employed a model-aided synthetic biology approach combined with microfluidics. We build and test excitable gene circuits designed to convert local chemical cues into synchronous bursts of PMP, thereby passing an electrical message to neighboring cells on extended spatial-temporal scales.

Results & Discussion

Briefly, our strategy includes a three-component gene circuit that controls potassium channel expression within the *S. cerevisiae* community following dynamic changes of chemical concentrations in the environment (Fig. 1A). Lately, we have found that chemical receptors from Mar family of antibiotic resistance genes[7] allow a direct interpretation of dynamic chemical environment into very robust gene expression patterns, synchronized across cell populations[8]. Therefore, we chose Mar receptors (consecutively named MarR and IacR) to facilitate dual-chemical perception of phytohormones salicylate acid (SA) and indole acetic acid/auxin (IAA) in the environment (Fig. 1B). Next, to encode excitability[9] we coupled IacR and MarR through positive and negative feedback loops in the dual-feedback synthetic gene circuit (Fig. 1B). To understand the dynamics of the designed circuit we first performed computer model simulations of the IacR-MarR feedback system to identify regimes that demonstrate the prominence for the excitable dynamics (Extended Data Fig. 1). Model predictions revealed minimal prerequisites for the transit between steady-state (Extended Data Fig. 1A), excitability (Extended Data Fig. 1B), and oscillations (Extended Data Fig. 1C). These conditions directly relate to the ratio of IacR-MarR deactivation (bifurcation point) which depends primarily on phytohormone concentrations in the environment (Extended Data Fig. 1A-C). Indeed, *in silico* periodic stimulations with IAA and SA predicted the sustained excitable response of the circuit triggered by phytohormones (Extended Data Fig. 1D).

To test experimentally model predictions, we implemented a synthetic circuit in *S. cerevisiae* by tagging IacR with herpes simplex virus trans-activation domain (VP64)[10] and MarR with repression Mig1 silencing domain[11] (Fig. 1B, Extended Data Fig. 2). Initially, we tested that this system responds to a broad range of IAA and SA concentrations in high-throughput time-lapse micro-well plate fluorescence assays (Extended Data Figs. 3 and 4). Next, we employed a controlled environment on the microfluidic chip where cells grow under continuous media perfusion (Fig. 1C and D). We stimulated dozens of engineered yeast populations with antithetic pulses of SA and IAA of either square or sine wave patterns with different frequencies to mimic

diverse environments. Throughout the experiment, we could control the period of stimuli with a microfluidic flow control system and record fluorescence changes of unstable dEGFP reporter[12] that reports the outcome of circuit dynamics (Supplementary Movie 1). Spatially coordinated oscillations of dEGFP were observed under phytohormone stimulation as rapid as 30 minutes (Fig. 1C, D, Extended Data Fig. 5A-D). The robust unison of cellular responses was confirmed further by the analysis of cumulative dEGFP signal autocorrelation (Fig. 1E), frequency response spectrum (Extended Data Fig. 6A), and period distribution (Fig. 1F). Typically, less than 5% shift in a phase were observed between colonies (Fig. 1G), indicative of global coordination among even distal fungi populations in both chemical microenvironments (sine or square-shaped waves) (Extended Data Fig. 5). Cell populations also exhibit a low dispersion (coefficient of variation (CV) < 1) of reporter amplitudes (Extended Data Fig. 6B), periods (Extended Data Fig. 6C), and peak widths (Extended Data Fig. 6D), indicative of high repeatability and robustness of transcriptional outcome.

In summary, the proposed chemically-excited circuit is an ideal system for the construction of the population-level chemical to the electrical signal converter.

The plasma membrane potential of yeast is regulated through voltage-gated potassium channels such as outward-rectifier channel TOK1[13,14]. TOK1 is the main target for several toxins and volatile anesthetic agents[15], which cause uncontrolled opening and leakage of potassium ions to the extracellular space. Overexpression of TOK1 causes membrane hyperpolarization (more negative PMP) while *tok1* mutation leads to membrane depolarization often accompanied by cell death[16]. Thereby, TOK1 controls potassium release from yeast cells and maintains a balance in the PMP. Next, we integrated our excitable circuit (Fig. 1A, B) to directly control the PMP by chemical modulation of ion channel transcription (Fig. 2A). Furthermore, to increase system modularity, the constitutively open KcsA bacterial potassium channel[17, 18] was successively used to replace the dEGFP reporter in the circuit (Fig. 2A). This modification aims in uncoupling voltage-dependent channel opening dynamics from the PMP assuring that the expression of the ion channel defines its activity based on changes of phytohormones in the environment (Fig. 2A). We measured PMP dynamics in yeast with a cationic dye Thioflavin T (ThT), previously used to correctly monitor PMP in yeast[19] and bacteria[3]. This dye shows a substantial increase in fluorescence following membrane hyperpolarization and its translocation to the cell interior acting as a Nernstian voltage indicator. A chemical potassium flux clamp experiment with the graded increase of KCL further confirmed the sensitivity and responsiveness of ThT dye as a PMP marker in yeast cells (Extended Data Fig. 7).

Growing engineered yeast in the microfluidic device subjected to different speeds of chemical stimuli revealed cyclic bursts of PMP (Fig. 2B, C) that were coordinated across populations (Fig 2B, C, and Extended Data Fig. 8A, and Supplementary Movies 2 and 3). However, this type of dynamics was not observed in the control yeast populations subjected to identical environmental fluctuations (Extended Data Fig. 8B, Supplementary Movie 4), indicating the chemically-excited circuit is indeed responsible for coordinated PMP bursts. Subsequent analysis of period distributions among colonies confirmed a dominant frequency of PMP firing that matched closely that of phytohormone stimulus (Fig. 2C). Similarly, cumulative autocorrelation (Fig. 2D) and frequency spectra (Fig. 2E) analyses confirmed robust coupling of PMP within and across distant populations. Furthermore, the relative variation of amplitudes, as well as period of PMP firings across colonies, was remarkably low (Extended Data Fig. 8C-F), indicating the effective passage

of electrical message within the population. Moreover, we evaluated the percentage of PMP phase drift between individual fungi populations and found very low phase differences (Fig. 2F) that strongly correlate with low variation of the period (Fig. 2 G and Extended Data Fig. 8E) again indicative of the robust electrical coupling between distant communities.

To further illustrate how coordinated electrical signals emerge from chemical stimuli in yeast consortia we developed a spatial-temporal computer model (Extended Data Fig. 9) that combines the excitable circuit (Fig. 2A) with Hodgkin–Huxley model of electrical signals(action-potentials)[20]. Model simulations of the populations (n=50) excited by a source cell show the robust propagation of PMP bursts across populations (Extended Data Fig. 9A). Moreover, the frequency of phytohormone changes in the environment similarly determines the population reaction speed to that observed in our experiments (Extended Data Fig. 9B). Therefore, experiments and model simulations explain how a chemically excitable cell can propagate the electrical message to its neighbors by dynamically modulating the expression of active potassium channels.

Finally, we tested whether our synthetic circuit (Fig. 1A) can be integrated with the host machinery to control native potassium channels. For that purpose, we wired our circuit to the transcription activation of the potent K1 killer toxin (Fig. 3A) that was suggested to act as the yeast TOK1 channel opener[21]. The strain producing K1 toxin in waves (Fig. 3A) was cocultured with a toxin-sensitive strain carrying empty plasmids, respectively (Fig. 3B). Our time-lapse experiments indicate that toxin-sensitive strain responds to waves of toxin dosage by adjusting PMP according to the frequency of K1 toxin production by killer strain (Fig. 3C-E, Supplementary Movie 5).

Thus, these findings demonstrate that PMP can be precisely controlled in the sender-receiver multi-strain consortia by hijacking host ion channels with rhythmic chemical control of volatile agents such as toxins or antibiotics in the environment.

In summary, we have identified a molecular mechanism underlying chemical to electrical signal conversion that coordinates entire microbial populations. We show that a chemically-excited circuit controls ion channels activity inside the microbial community allowing equal charging(hyperpolarization) of individual cells. Such a “battery-mimicking” mechanism is robust to the presence of cellular noise and environmental fluctuations, as it processes local chemical signals with high precision through host transcriptional machinery. By analogy, one could think about this type of converter mechanism as a functional counterpart of electrical-chemical conversion mediated by neurons. Thus, this work in addition to serving as a compact model for understanding chemical-electrical signal conversion in cell communities, it opens new avenue in the field of synthetic biology by enabling an effective transformation of chemical cues into an evenly disturbed electrical signal network in virtually any biological setup, including microbial biofilms as well as multicellular organisms.

References

1. L. Aron, B. A. Yankner, Neural synchronization in Alzheimer’s disease. *Nature*. **540**, 207–208 (2016).

2. T. Masatsugu, S. Dirk, S.-T. Satoe, J. Wang, Z. Tong, K. A. J., H. G. A., G. Simon, Glutamate triggers long-distance, calcium-based plant defense signaling. *Science (80-.).* **361**, 1112–1115 (2018).

3. A. Prindle, J. Liu, M. Asally, S. Ly, J. Garcia-Ojalvo, G. M. Süel, Ion channels enable electrical communication in bacterial communities. *Nature*. **527**, 59–63 (2015).

4. D. D. A., C. J. Morais, P. R. A., K. Anling, G. J. M., C. S. L., C. B. T., M. Roderick, The Structure of the Potassium Channel: Molecular Basis of K+ Conduction and Selectivity. *Science (80-.).* **280**, 69–77 (1998).

5. D. Debanne, N. C. Guérineau, B. H. Gähwiler, S. M. Thompson, Action-potential propagation gated by an axonal IA-like K+ conductance in hippocampus. *Nature*. **389**, 286–289 (1997).

6. B. Naundorf, F. Wolf, M. Volgushev, Unique features of action potential initiation in cortical neurons. *Nature*. **440**, 1060–1063 (2006).

7. Will, W. R. & Fang, F. C. The evolution of MarR family transcription factors as counter-silencers in regulatory networks. *Curr. Opin. Microbiol.* **55**, 1–8 (2020).

8. Pérez-García, S. *et al.* Synchronization of gene expression across eukaryotic communities through chemical rhythms. *Nat. Commun.* **12**, 4017 (2021).

9. Lindner, B., Garcia-Ojalvo, J., Neiman, A. & Schimansky-Geier, L. Effects of noise in excitable systems. *Phys. Rep.* **392**, 321–424 (2004).

10. M. Hagmann, O. Georgiev, W. Schaffner The VP16 paradox: herpes simplex virus VP16 contains a long-range activation domain but within the natural multiprotein complex activates only from promoter-proximal positions *J. Virol.* 71, 5952–5962 (1997).

11. Ostling, J., Carlberg, M. & Ronne, H. Functional domains in the Mig1 repressor. *Mol. Cell. Biol.* **16**, 753 LP-761 (1996).

12. Dantuma, N. P., Lindsten, K., Glas, R., Jellne, M. & Masucci, M. G. Short-lived green fluorescent proteins for quantifying ubiquitin/proteasome-dependent proteolysis in living cells. *Nat. Biotechnol.* **18**, 538–543 (2000).

13. Martinac, B., Saimi, Y. & Kung, C. Ion channels in microbes. *Physiol. Rev.* **88**, 1449–1490 (2008).

14. Mackie, T. D. & Brodsky, J. L. Investigating Potassium Channels in Budding Yeast: A Genetic Sandbox. *Genetics* **209**, 637–650 (2018).

15. Ahmed, A. *et al.* A Molecular Target for Viral Killer Toxin TOK1 Potassium Channels. *Cell* **99**, 283–291 (1999).

16. Sesti, F., Shih, T., Nikolaeva, N. & Goldstein, S. Immunity to K1 killer toxin: Internal TOK1 blockade. *Cell* **105**, 637–644 (2001).

17. Cuello, L. G. *et al.* Design and characterization of a constitutively open KcsA. *FEBS Lett.* **584**, 1133–1138 (2010).

18. Sun, Z., Xu, Y., Zhang, D. & McDermott, A. E. Probing allosteric coupling in a constitutively open mutant of the ion channel KcsA using solid-state NMR. *Proc. Natl. Acad. Sci.* **117**, 7171 LP-7175 (2020).

19. Peña, A., Sánchez, N. & Calahorra, M. In: Membrane Potential: An Overview ESTIMATIONS AND ACTUAL MEASUREMENTS OF THE PLASMA MEMBRANE ELECTRIC POTENTIAL DIFFERENCE IN YEAST. in 81–104 (2020).

20. Ambrosio, B., Aziz-Alaoui, M. A. & Balti, A. Propagation of Bursting Oscillations in Coupled Non-homogeneous Hodgkin–Huxley Reaction–Diffusion Systems. *Differ. Equations Dyn. Syst.* (2017) doi:10.1007/s12591-017-0366-6.

21. Carroll, S. Y. *et al.* A yeast killer toxin screen provides insights into a/b toxin entry, trafficking, and killing mechanisms. *Dev. Cell* **17**, 552–560 (2009).

22. Alekshun, M. N., Levy, S. B., Mealy, T. R., Seaton, B. A. & Head, J. F. The crystal structure of MarR, a regulator of multiple antibiotic resistance, at 2.3 A resolution. *Nat. Struct. Biol.* **8**, 710–714 (2001).

23. Shu, H.-Y. *et al.* Transcriptional regulation of the iac locus from Acinetobacter baumannii by the phytohormone indole-3-acetic acid. *Antonie Van Leeuwenhoek* **107**, 1237–1247 (2015).

24. Takeuchi, J., Chen, H., Hoyt, M. A. & Coffino, P. Structural elements of the ubiquitin-independent proteasome degron of ornithine decarboxylase. *Biochem. J.* **410**, 401–407 (2008).

25. A. L. HODGKIN, A. F. HUXLEY, A quantitative description of membrane current and its application to conduction and excitation in nerve. *J. Physiol.* **117**, 500–544 (1952).

Acknowledgments

We would like to thank Dr. Luis Rubio for providing BY4741 laboratory yeast strain used in this work. This work was supported by the Programa de Atraccion de Talento 2017 (Comunidad de Madrid, 2017-T1/BIO-5654 to K.W.), Severo Ochoa (SO) Programme for Centres of Excellence in R&D from the Agencia Estatal de Investigacion of Spain (grant SEV-2016-0672 (2017-2021) to K.W. via the CBGP). In the frame of SEV-2016-0672 funding M.A. received a PhD fellowship (SEV-2016-0672-18-3: PRE2018-084946). K.W. was supported by Programa Estatal de Generacion del Conocimiento y Fortalecimiento Científico y Tecnologico del Sistema de I+D+I

2019 (PGC2018-093387-A-I00) from MICIU (to K.W.). UPM Plan Propio Predoctoral fellow finances M.G.N

Author contributions

M.G.N, S.P.G, and M.A. designed, performed most of the experiments, and analyzed data. D.R.S, contributed to plasmid and strain constructions, S.P.G and M.A, performed multi-well plate fluorescence assays. K.W designed experiments analyzed data and supervised the project. All authors contribute to the manuscript writing.

Competing interests

Authors declare that they have no competing interests.

Data and materials availability

All data are shown in the main text or the supplementary materials. Plasmids and strains are available upon request from authors.

Methods

1.1 Strains and plasmid constructions

Constructs were cloned using isothermal Gibson assembly cloning. A middle-copy (~10-30 copies) episomal plasmid pGADT7 (Takara Bio Inc.) was used to increase the concentration of proteins to buffer for the effects of intrinsic molecular noise and selected using different auxotrophic selection markers (Leucine, Uracil, and Histidine). $Iacr_o$/$MarR_o$ promoter and either standard CYC1 or ADH1 yeast terminators were cloned into activator or repressor plasmids (Extended Data Fig. 2A). MarR and IacR were codon-optimized for yeast and synthesized using services delivered by Integrated DNA Technologies (IDT). The reporter plasmids include synthetic minimal promoters (synthesized with IDT) with previously identified MarR or IacR operator[22,23] sequences upstream TATA-box and minimal CYC1 promoter and fast-degradable UBG76V-EGFP (dEGFP)[12]. KcsA bacterial potassium channel was engineered to include open configuration mutations as previously described[17,18] and modified further to include plasma membrane localization signals and c-terminus mouse ODC degron signal[24].
K1 toxin was codon-optimized and synthesized throughs IDT. KcsA* and K1 toxin replace the dEGFP gene on the reporter plasmid, respectively (Extended Data Fig. 2B).
PCR reactions were performed using Q5 high fidelity polymerase (New England Biolabs). Correct PCR products were digested with DpnI (New England Biolabs) to remove the template and subsequently cleaned up with a DNA cleanup kit (Zymo Research) before Gibson assembly. Constructs were transformed in ultra-competent cells from E. coli DH5a strain using standard protocols. All plasmids were confirmed by colony PCR and validated with sequencing. The BY4741 laboratory yeast strain (a kind gift from Dr. Luis Rubio) carrying integrated copy constitutively expressed mCherry reporter was used to prepare competent cells and transformation of plasmids using Frozen-EZ Yeast Transformation II Kit (Zymo Research). Sequences of oligos and synthetic DNA used in this study are shown in Data S1.

1.2 Multiwell plate and microscopy fluorescence measurements

Overnight culture of the yeast grown in 2% sucrose low fluorescence media (Formedium, UK) was diluted 100x and pipetted directly to a 96 well plate containing 2% sucrose and gradient of SA and IAA concentrations. Plates were incubated at 30C overnight and well mixed by shaking before performing measurements. Measurements were done with the Thermo Scientific™ VarioskanTM LUX multimode microplate reader after 24h or were recorded every 10min to generate a time-lapse profile of the dEGFP and OD600. OD600 was set at an absorbance of 600nm wavelength, the fluorescence excitation and emission light at 488nm and 517nm wavelength for dEGFP.
The PMP reporter activity was analyzed by measuring Thioflavin (ThT) expression using potassium clamp experiments. Overnight cultures were diluted to a total OD600 of 0.1. KCL at different concentrations was added to the diluted cultures. Aliquotes of 200 µL were pipetted from these diluted cultures to a multi-well plate containing different KCL concentrations (0 mM, 50mM, 100mM, 200mM, and 400mM) and 10uM Thioflavin T. Plates were incubated at 30 °C overnight. The next day each well was imaged in two different channels: differential interference contrast (DIC) and GFP (λEx = 488 nm; λEm = 515 nm). The image acquisition was controlled by the software µManager and Leica DMI9 and images were captured using a 10x dry objective (NA=0.32).

1.3 Time-lapse imaging, growth conditions, and data analysis

Live-cell imaging was performed on the Automated inverted Leica DMi8 fluorescence microscope equipped with Hamamatsu Orca Flash V3 camera that was controlled by Micro-Manager v.2.0 (https://micro-manager.org/). Images were captured with 40x dry objective NA=0.8 (Leica Inc.). Traps containing cells were imaged every 10 minutes on three different channels (DIC, GFP (Excitation: 488 Emission: 515, and mCherry Excitation: 583, Emission: 610) with CoolLed pE600 LED excitation source and standard Chroma epifluorescent filter set. Experiments were run for up to 72 hours under the continuous supply of nutrients in the microfluidic device. Acquired images were initially processed in Fiji 2.0 (https://imagej.net/Fiji) using custom scripting to extract positions with exponentially growing yeast cells. Constitutively expressed mCherry marker was used to identify exponentially growing cells and used to derive normalized dEGFP fluorescence: Dead or non-growing individuals were discarded by correcting dEGFP signal according to the formula $dEGFP/(dEGFP + mCherry)$ or alternatively K1 toxin producing strain.
Each image was divided into 25 regions of interest (ROIs) and analyzed separately to isolate regions where cells were actively growing and could be tracked over time. The posterior analysis was done with custom R-studio scripts. Firstly, raw data were detrended using the detrend function from "pracma" R-studio v4.0.3 package and then smoothed with Savitzky-Golay Smoothing function (savgol), from the same package, with a filter length of 15 was applied and the signal was normalized between 0 and 1 to generate heatmaps across cell traps. Amplitudes were calculated with find peaks within the Process Data using the "findpeaks" function from "pracma" R package with nups and ndowns of 6, and periods were calculated by calculating distances between successive dEGFP peaks. Phase drift was calculated by comparing time differences of successive dEGFP peaks between cell communities in a microfluidic device to derive inter-community measures. Cumulative autocorrelations traces and power spectrum densities were calculated on mean dEGFP trajectories per colony calculated for n-communities (n>20, ~20,000 cells) using

standard calculations with Matlab 2018b derived packages autocorrect and Fast Fourier Transformation (FFT). The same procedure was used to evaluate ThT fluorescence dynamics, autocorrelation function and frequency responses.

1.4 Mathematical model descriptions

To derive a mathematical model of the excitable circuit (Fig. 1B) we used a system of coupled ordinary differential (ODE) equations adapted from previous theoretical studies[9]. Briefly, IacR and MarR protein concentrations change over time according to the following formulas:

$$\frac{\partial IacR}{\partial t} = a_1 + \frac{b_1 \cdot IacR^2}{K_A^2 + IacR^2 + (\gamma \cdot MarR)^2} - d_1 \cdot (1 + \epsilon_I \cdot IAA) \cdot IacR \quad (1)$$

$$\frac{\partial MarR}{\partial t} = a_2 + \frac{b_2 \cdot IacR^2}{K_B^2 + IacR^2} - d_2 \cdot (1 + \epsilon_M \cdot SA) \cdot MarR \quad (2)$$

where a_1 and a_2 are basal IacR and MarR production rates. b_1 and b_2 are IacR-dependent protein production rates. K_A and K_B are half-max hill function coefficients, and γ is the rate of MarR-dependent repression. d_1 and d_2 are protein turnover rates, respectively. ϵ_I and ϵ_M are the rates of phytohormone effect on a total protein turnover. IAA and SA are modeled using square wave and sine signal generators (Matlab Inc.).

The ratio of protein turnover $\frac{d_1}{d_2}$ (Extended Data Fig. 1A-C) represents a key bifurcation parameter that enables the transition of the system into oscillatory and excitable regimes.

To calculate nullclines we set the left-hand side of Eqs. 1 and 2 to 0 and setting ϵ_I and ϵ_M to 0. One can derive the following terms for calculation of phase portraits MarR*(IacR) and MarR**(IacR) (Extended Data Fig. 1A-C):

$$MarR^* = \frac{1}{\gamma} \cdot \sqrt{-\frac{K_A^2 \cdot a_1 + a_1 \cdot IacR^2 + b_1 \cdot IacR^2 - d_1 \cdot IacR^3 - K_A^2 \cdot d_1 \cdot IacR}{a_1 - d_1 \cdot IacR}} \quad (3)$$

$$MarR^{**} = \frac{a_2 + \frac{b_2 \cdot IacR^2}{K_B^2 + IacR^2}}{d_2} \quad (4)$$

The spatial-temporal PDE model of PMP firings (Extended Data Fig. 9) was simulated using space discretization dx of one colony unit. The IacR and MarR were modeled using indexed eqs. 1 and 2 $IacR_i$ and $MarR_i$ where I is yeast population index i=1…N , N=50.

The Hodgkin–Huxley[25] plasma membrane potential P_i for the ith population changes over time as follows:

$$\frac{\partial P_i}{\partial t} = g_k \cdot {CH_i}^4 \cdot (P_K - P_i) + g_L \cdot (P_L - P_i) + \phi \cdot (P_{i+1} + P_{i-1} - 2 \cdot P_i) \quad (5)$$

whereas the potassium channel species in the ith population (CH_i)are written as:

$$\frac{\partial CH_i}{\partial t} = a_1 + \frac{b_1 \cdot IacR^2}{K_A^2 + IacR^2 + (\gamma \cdot MarR)^2} + a_3 \cdot \alpha \cdot (1 - CH_i) - d_3 \cdot \beta \cdot CH_i \quad (6)$$

$\alpha = 0.01 \cdot \frac{-P_i+10}{e^{1-0.1 \cdot P_i}-1}$ and $\beta = 0.125 \cdot e^{-P_i/80}$
where g_k is electric current constant for potassium ions (channel conductance) and g_L is a general leak current constant, respectively. P_K and P_L are resting membrane potentials. The parameter ϕ denotes the rate of potassium exchange between populations that balances PMP. Parameters a_3 and d_3 depict activation and turnover rates of the ion channel. Model parameters are summarized in Supplementary Table 1.

1.5 Cell loading procedure

All tubing lines were sterilized with ethanol and plugged into syringes or introduced in falcon tubes under sterile conditions. Fresh yeast colony was grown in low fluorescence media composition (Formedium, UK) with 2% sucrose as a carbon source or 2% glucose (K1 toxin-producing strain). The next day, yeast cultures were diluted 10-20 times approximately to 0.2-0.4 O.D600 to obtain highly concentrated cells that were transferred to a 50mL falcon tube for loading. 60mL media syringes were filled with 25mL of inducing media (2% sucrose + 0.5%galactose) with or without compounds and 50mL waste falcons tubes were filled with 10mL of DDI water. Before loading, devices were vacuumed for at least 20 minutes to remove all the air from the channels and traps. Syringes and falcon tubes were placed on the height control system and lines were connected as follows; media syringes were plugged first and kept above all other inputs to prevent media contamination. Adjusting the height of the cells-containing falcon tube as well as media and waste aids in controlling the cell seeding in the traps. Although many cells pass through the chip directly towards the waste port, few cells got captured via microvalves and seeded the traps. Once 10-20 cells were captured in each trapping region, the flow from the cell loading port was reverted by decreasing the height to the same level as for the auxiliary waste.

1.6 Microfluidic Mold fabrication

Molds for the production of microfluidic device[8] were designed in Inkscape and printed on plastic sheets with the monochrome laser printer at 1200dpi resolution as described in [8]. A density of Ink deposition was used to control the feature height. Plastic wafers were cut and transferred to the thermal oven set to 160ºC to shrink by one-third of the original size, then baked again for 10 min to smoothen and harden the ink. Finally, molds were cleaned with soap, rinsed with isopropanol and DDI water and dried using a nitrogen gun, and secured with Scotch tape before use.

1.7 Soft Lithography

Molds were introduced in plastic 90mm Petri dishes and fixed with double-sided tape. Dowsil Sylgard 184 Polydimethylsiloxane (PDMS) was properly mixed in a 10:1 (w/w) ratio of elastomer and curing agent and stirred until the uniform consistency was achieved. Approximately 27mL of the homogeneous mixture was poured into each petri dish and completely degassed using the 8 CFM 2-stage vacuum pump for approximately 20 minutes. Degassed PDMS was cured at 80oC for 2h. Cured PDMS was removed from the petri dish, separated from the wafer, and cut to extract the individual chips. Fluid access ports were punched with a 0.7mm diameter World Precision Instruments (WPI) biopsy puncher and flushed with ethanol to remove any remaining PDMS.

Individual chips were cleaned with ethanol and DDI water and Scotch tape to remove any remaining dirt particles.

1.8 Microfluidic device bonding

At least one day before use, individual chips and coverslips were cleaned in the sonic bath and rinsed in ethanol, isopropanol, and water. Both surfaces were exposed to Corona SB plasma treater (ElectroTechnics Model BD-20AC Hand-Held Laboratory Corona Treater) between 45 seconds to 1 minute, then surfaces were brought together and introduced at 80ºC in an oven overnight to obtain the enhanced bond strength.

Figures

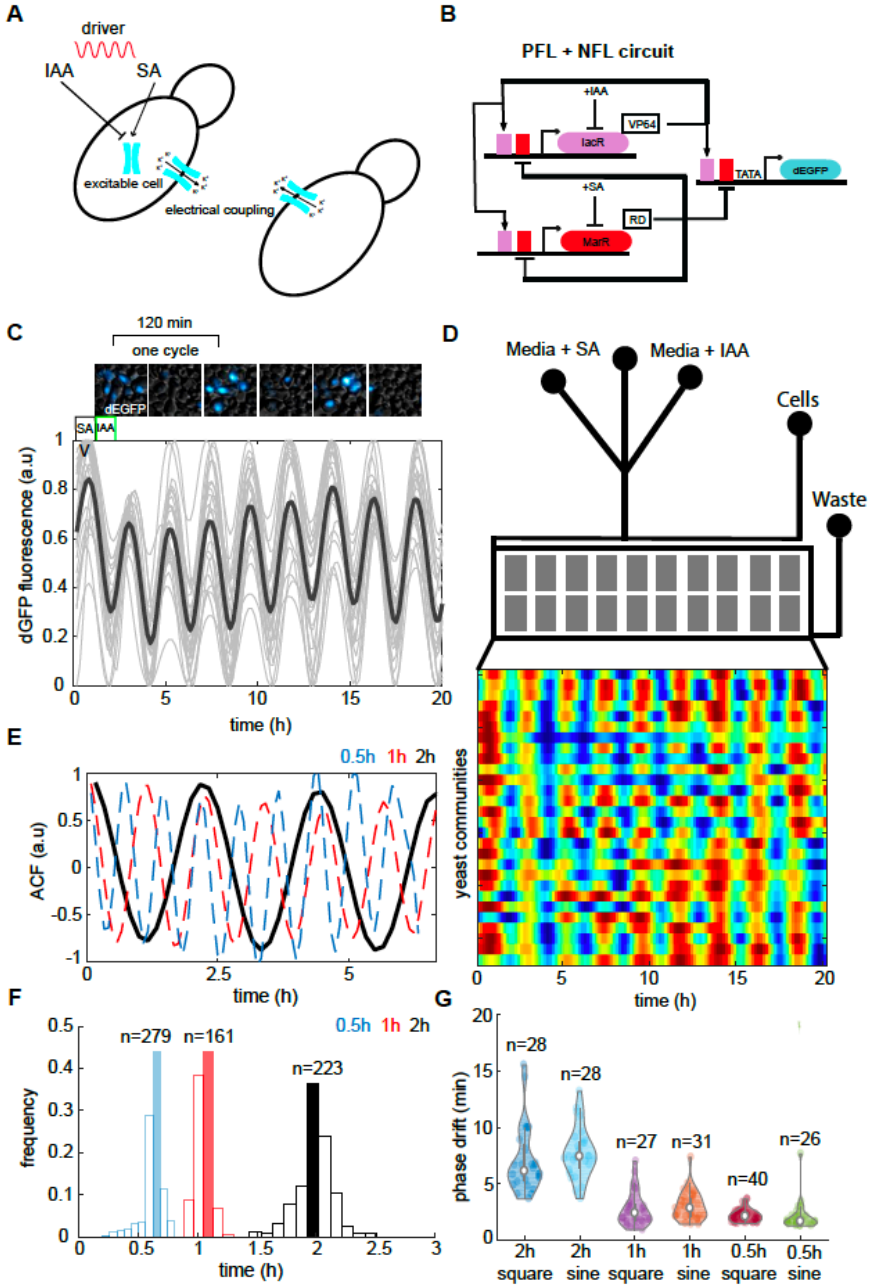

Fig. 1. Experimental validation of excitable circuit model driven by IAA-SA environmental clocks

(A, B) A prototype scheme of the chemical-electrical signal converter. Two phytohormones IAA and SA control the transcription of the potassium channel (cyan) through coupled positive and negative feedback circuits (B). IacR sensor acts as an activator in a positive feedback loop (PFL) and MarR is a repressor in the negative feedback loop (NFL). dEGFP reporter is a short-lived EGFP protein placed under the control of IacR/MarR regulated promoter. Each cell is interfaced with the environment through the detection of IAA-SA stimuli, eventually resulting in the

electrical signal coupling within the consortia. **(C)** Top panel, sample screenshots from microfluidic experiments with cells carrying excitable circuits (B). Bottom panel, dEGFP time traces from all traps recorded in the microfluidic device show distinct peaks of dEGFP fluorescence. **(D)** Schematics of the microfluidic device (top panel) with input and output ports and cell trapping regions, and heat map of dEGFP fluorescence for each of recorded trapping regions (n=28 yeast communities) corresponds to time traces(C). Note the complete synchrony between individual cell traps (n=26, 27, 28). (**E**) Cumulative auto-correlation function (ACF) of dEGFP reporter for all recorder population trapping regions recorded for three different periods of IAA-SA environmental stimuli. (**F**) Observed frequencies of periodic dEGFP response. The period of dEGFP oscillations is matched across yeast communities as shown by sharp period distributions. **(G)** Minimal phase drift (~5%) indicates remarkable coordination across populations of cells, regardless of phytohormone clock period or shape of environmental stimulus.

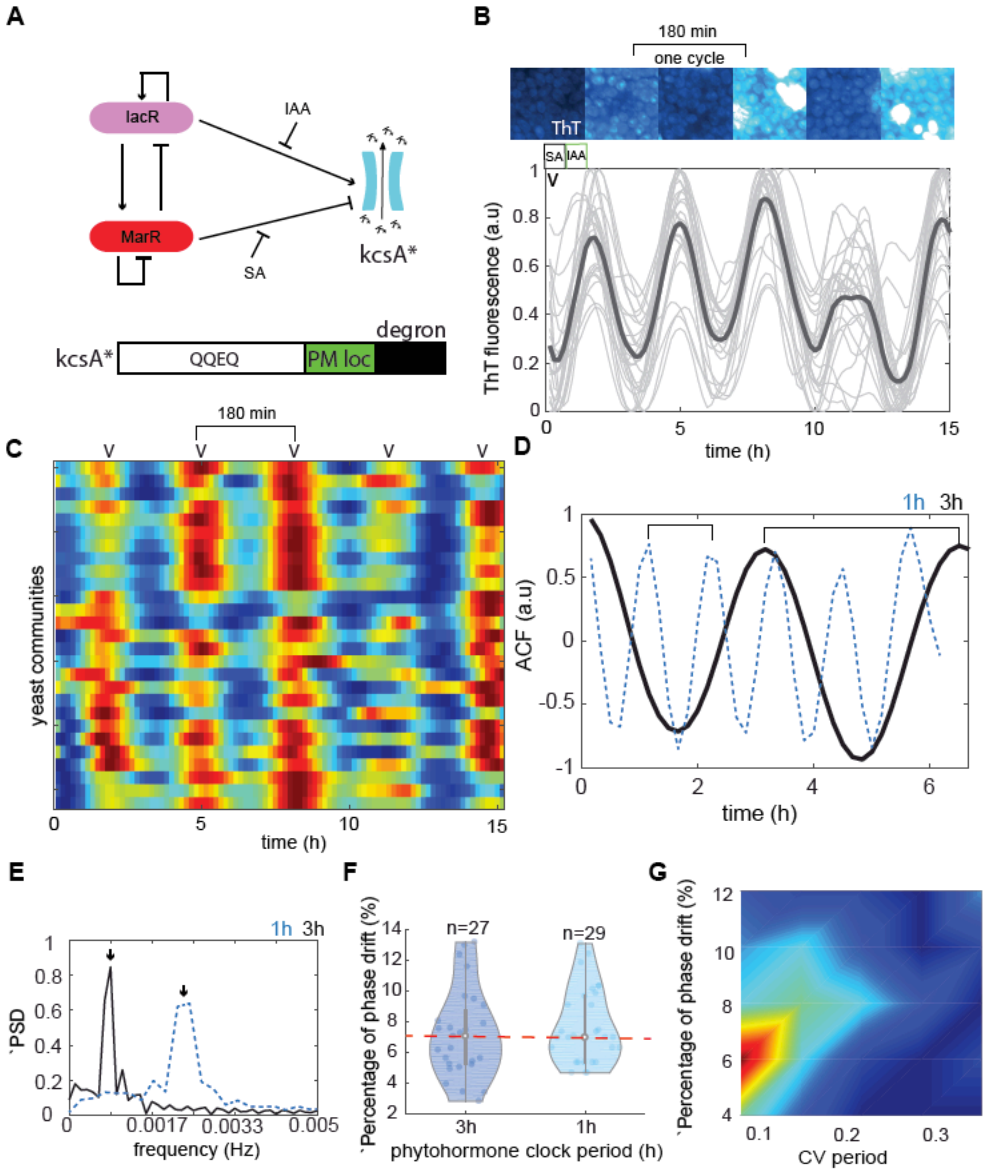

Fig. 2. An experimental model of the electrochemical system with a dual feedback circuit to genetically control electrical signals within cell communities.

(A) Schematics of the chemical-electrical converter system contain a dual feedback module (Fig. 1B) that controls the potassium channel activity (KcsA*, lower panel). KcsA* is a constitutively open bacterial potassium channel with plasma membrane localization (PM loc, green) and c-terminus mouse ODC degron (degron, black) sequences. **(B)** Screenshots and time traces from microfluidic experiments display successive cycles of PMP bursts by recording the ThT fluorescence. The period of the IAA-SA environmental clock was set to 3 hours. **(C)** a heat map of ThT fluorescence across all recorded yeast communities corresponds to time traces (B). **(D)** The comparison of cumulative auto-correlation (ACF) of ThT fluorescence for 1 hour (blue dash line) and 3 hours (black line)phytohormone stimulation periods. Note the clear periodic pattern of PMP changes synchronized across populations (**E**) ThT Frequency spectra (PSD) of globally coordinated populations for 1-hour (blue dash line), and 3-hour (black line) phytohormone stimuli. (**F**) The percentage of oscillatory drift as the function of the phytohormone stimuli period. Note

that 93% of recorder yeast colonies show the same timing of PMP firings with the speed that is dependent on phytohormone rhythms. (**G**) Density plot of phase drift percentage in the function of ThT period CV. Note a strong correlation between tight coordination of ~93% yeast communities(red cluster) and low variance of ThT period.

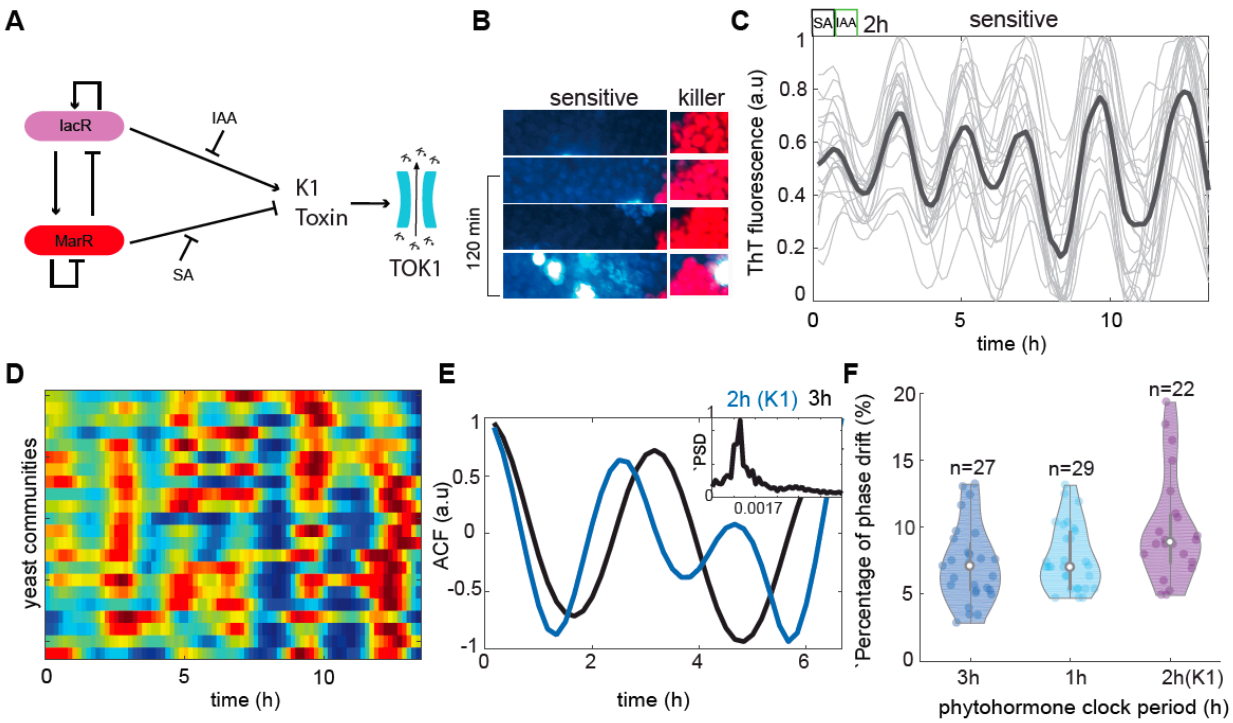

Fig. 3. Synchronous electrical signaling modulation through the integration with host machinery and volatile agents.

(A) Schematics of electrical signal modulation via integration with the host potassium channel. The excitable circuit (Fig. 1B) controls K1 toxin production. The toxin is released to extracellular space and activates TOK1 channel-dependent potassium flux. (**B**) Example screenshots from co-culture experiments of toxin-producing (mCherry) and sensitive (ThT) strains in the microfluidic device. (**C**) ThT time traces from all traps recorded in the microfluidic device show distinct peaks of PMP potential. (**D**) Heatmap of ThT dynamics in all recorder traps. (**E**) Comparison of cumulative autocorrelation between KcsA* circuits (Fig. 2A) and K1 circuits (A). In both scenarios, a clear oscillatory trend can be observed. The frequency response of the K1-based circuit is presented in the top panel. (**F**) A coordination of PMP firings at inter-community level (phase drift percentage) in the KcsA system (3h, 1h stimuli), and K1-based system (2h stimulus) varies between 90% to 94%.

Extended Data Figures

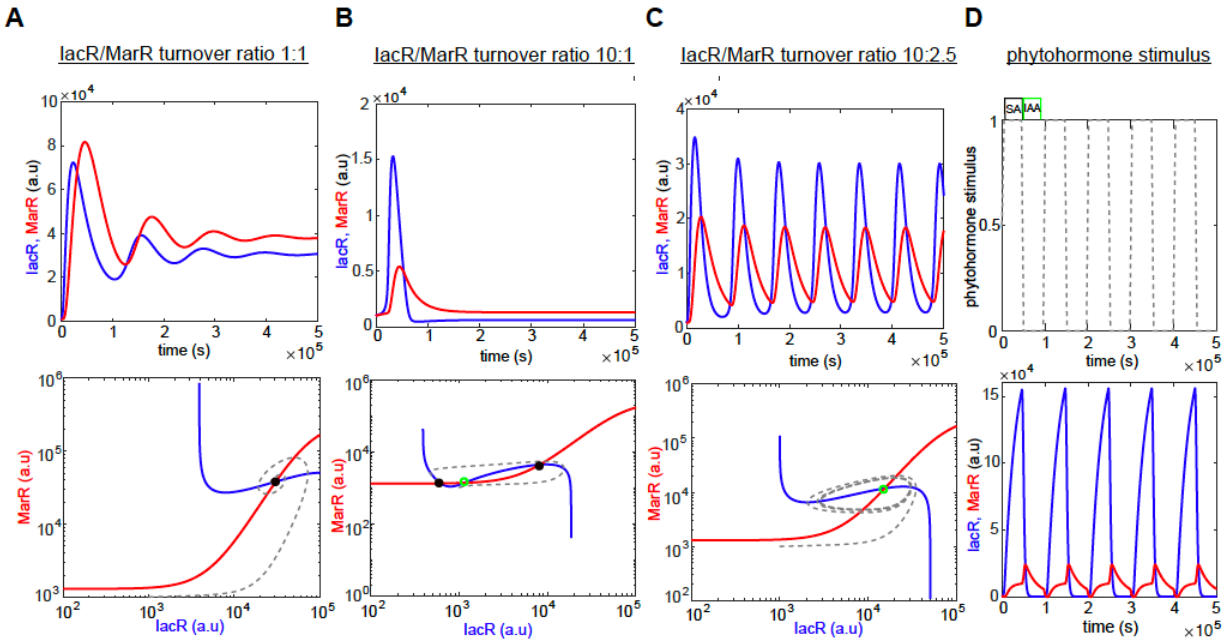

Extended Data Fig. 1. Computer model simulations of IacR-MarR feedback circuit reveal excitable dynamics controlled by phytohormones.

(A-C) Computer simulations of a dual-feedback circuit model (upper panel) and corresponding phase portraits with nullclines (lower panel) for the different ratio of IacR-MarR receptor turnover (1:1 (A), 10:1 (B), 10:2 (C)). Stable states are marked with black-filled circles and unsteady states with a green empty circle, respectively. Note that a higher turnover ratio produces the transition into an excitable regime around the unstable state(B). **(D)** Environmental phytohormone stimuli push the system into an excitable regime by directly increasing and successively decreasing the IacR-MarR turnover ratio(B).

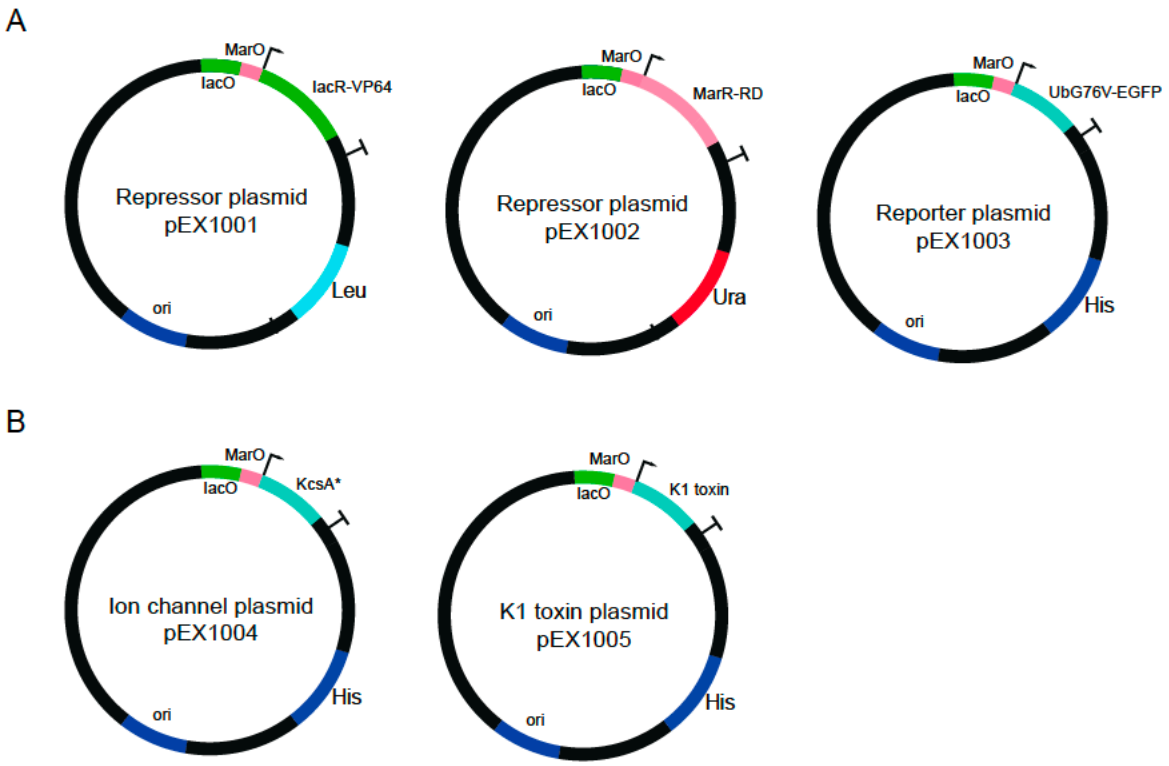

Extended Data Fig. 2. The plasmids used in the study.

(A, B) Plasmid map schematics were used in the study. (A) Activator (IacR) and repressor (MarR) and reporter (dEGFP) plasmids were used to build an excitable circuit as shown in Fig. 1B. (B) Additional plasmids are used to construct an electrical signaling mediator; an engineered ion channel (KcsA*) or host interface (K1 toxin).

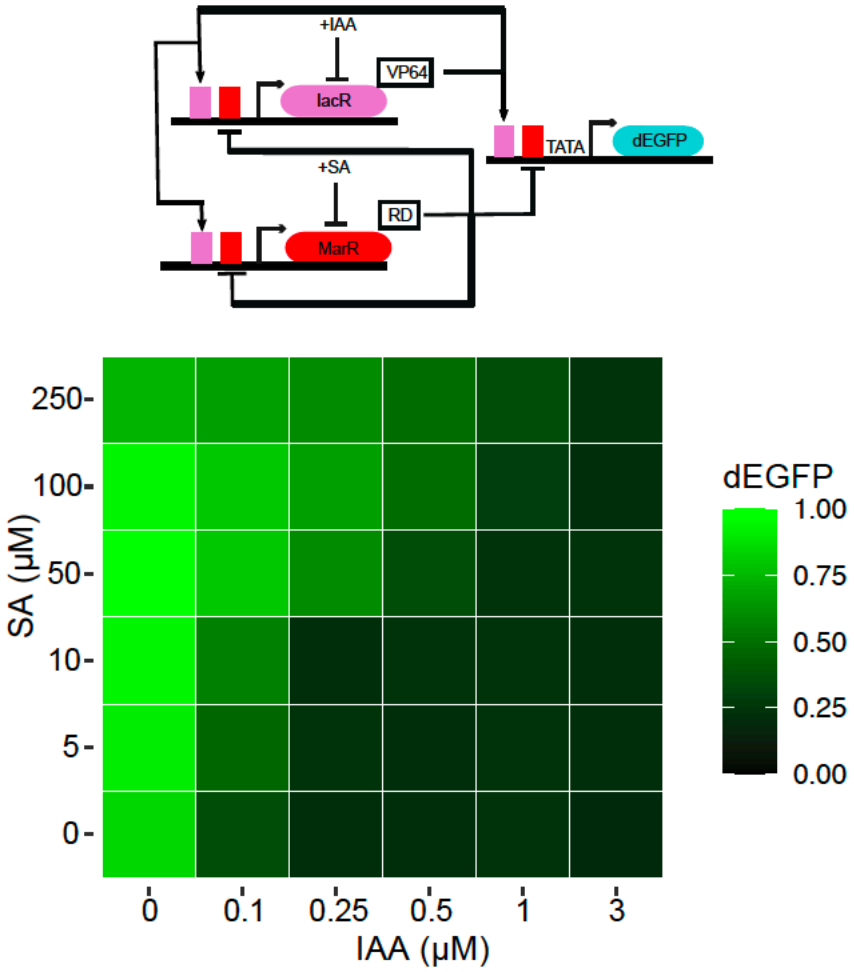

Extended Data Fig. 3. Precise control of circuit output with dual phytohormones.

A heat map of excitable circuit response recorder with dEGFP reporter (upper panel) to chemical gradients (lower panel). Note a precise control of circuit output is possible by using a dual phytohormone strategy. Mean measurements from three biological replicates (n=3) are shown.

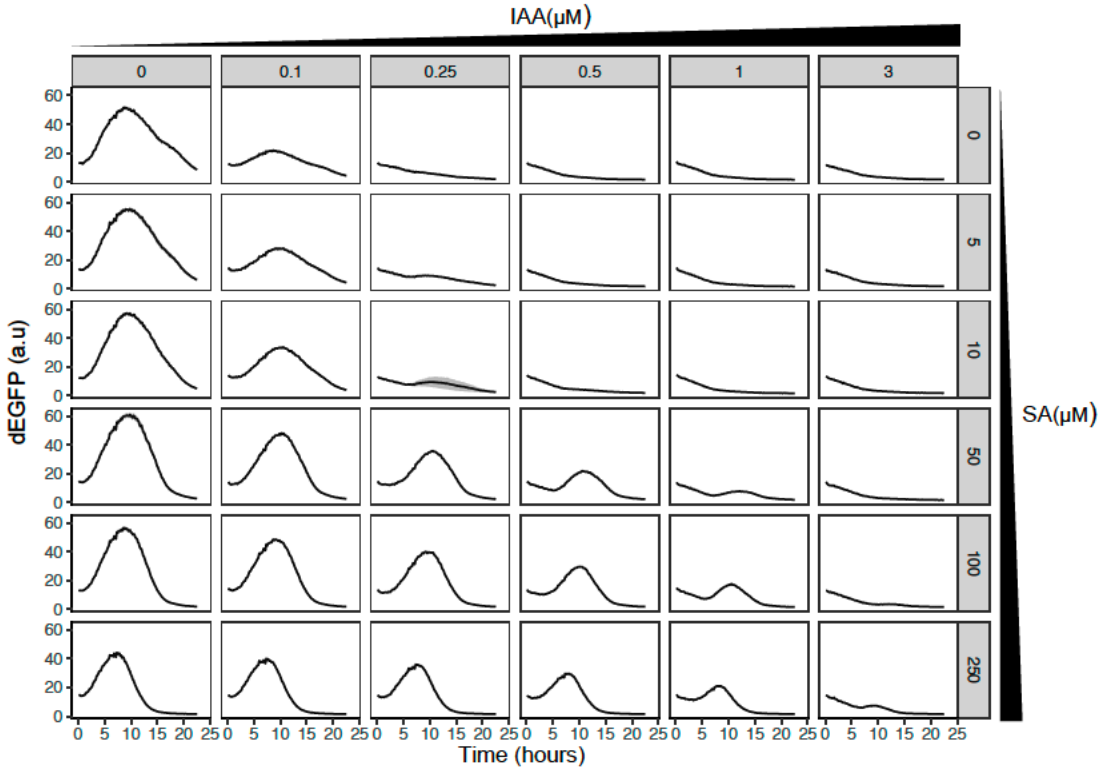
IAA(μM)
0
0.1
0.25
0.5
1
3
SA(μM)
0
5
10
50
100
250
dEGFP (a.u)
Time (hours)

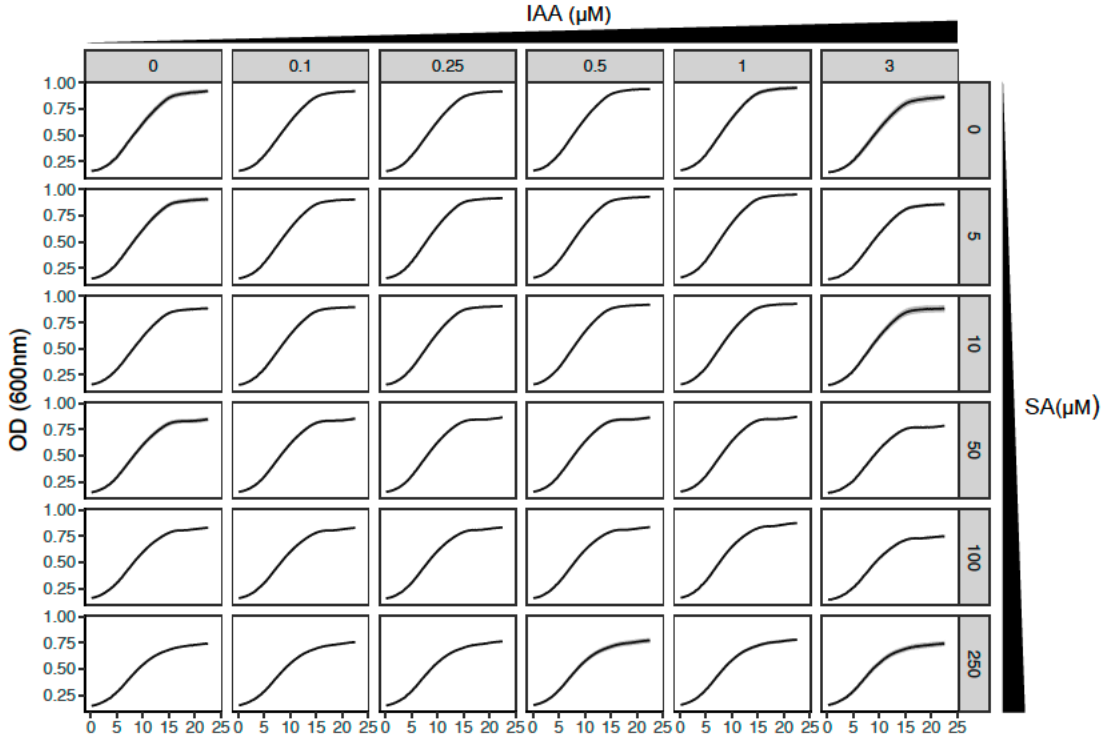
IAA (μM)
0
0.1
0.25
0.5
1
3
SA(μM)
0
5
10
50
100
250
OD (600nm)

Extended Data Fig. 4. Time-lapse synthetic circuit characterization using high-throughput fluorescence assays.

dEGFP fluorescence normalized to OD600 (upper panel) and OD600 absorbance (lower panel) for 24-hour measurements using graded changes of phytohormones was used to analyze the excitable potential of the synthetic circuit. Mean measurements with variations(shaded regions) from three biological replicates (n=3) are shown.

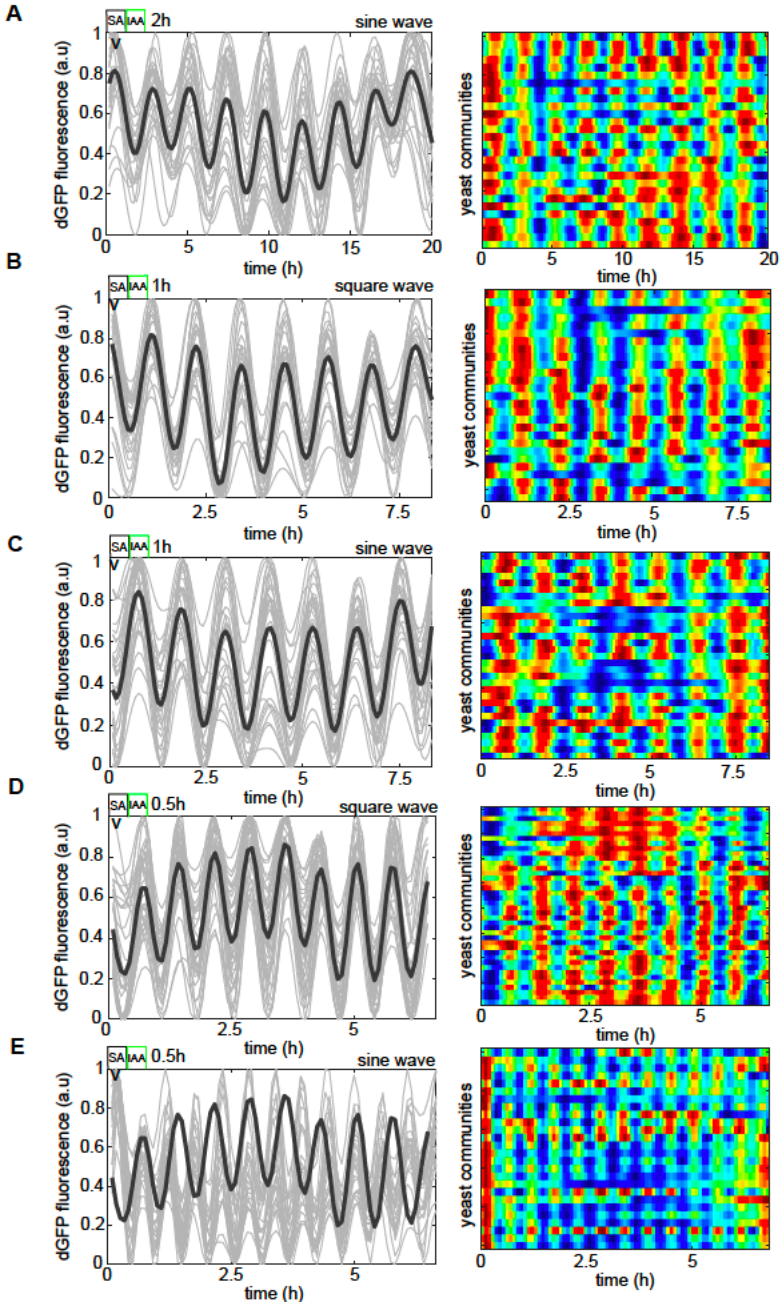

Extended Data Fig. 5. The frequency of phytohormone stimuli determines the excitable dynamics of the reporter gene under different types of environmental drivers.

(A-E) Left panel, dEGFP time evolutions from all traps recorded in the microfluidic device. Right panel, the heat map of dEGFP fluorescence for each of the recorded trapping regions corresponds to time traces(left panel). (A), Periodic 2-hour phytohormone wave of sine shape, (B, C) 1-hour periodic waves of square(B) and sine (C) shapes. (D, E) 30 min periodic wave of square (D) and sine (E) shapes, respectively. Note that the frequency of dEGFP firings mirrors exactly that of the chemical microenvironment. Color coding is as in Fig. 1.

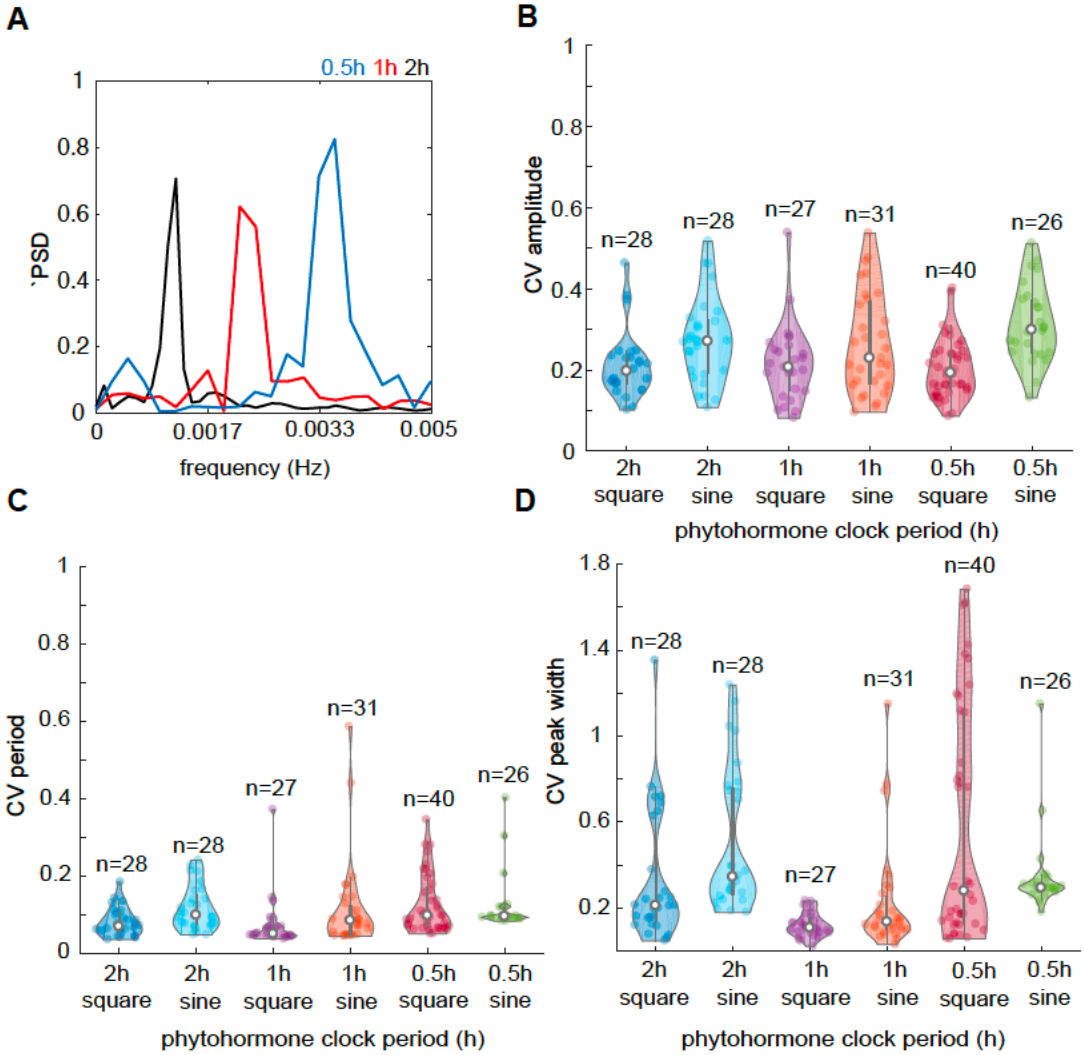

Extended Data Fig. 6. The excitable circuit shows low variation in the period, amplitude, and response peak width regardless of the stimulation period.

(A) dEGFP Frequency spectra (PSD) of globally coordinated populations for different periods of phytohormone rhythms (2h, 1h, and 30min respectively). (**B-D**) Coefficients of variation (CV) in the amplitude(B), periods(C), and response peak width(D) of dEGFP fluorescent reporter under different environments and stimulus periods. Note generally very low CV (CV < 1) indicates low variation in dEGFP reporter signal characteristics.

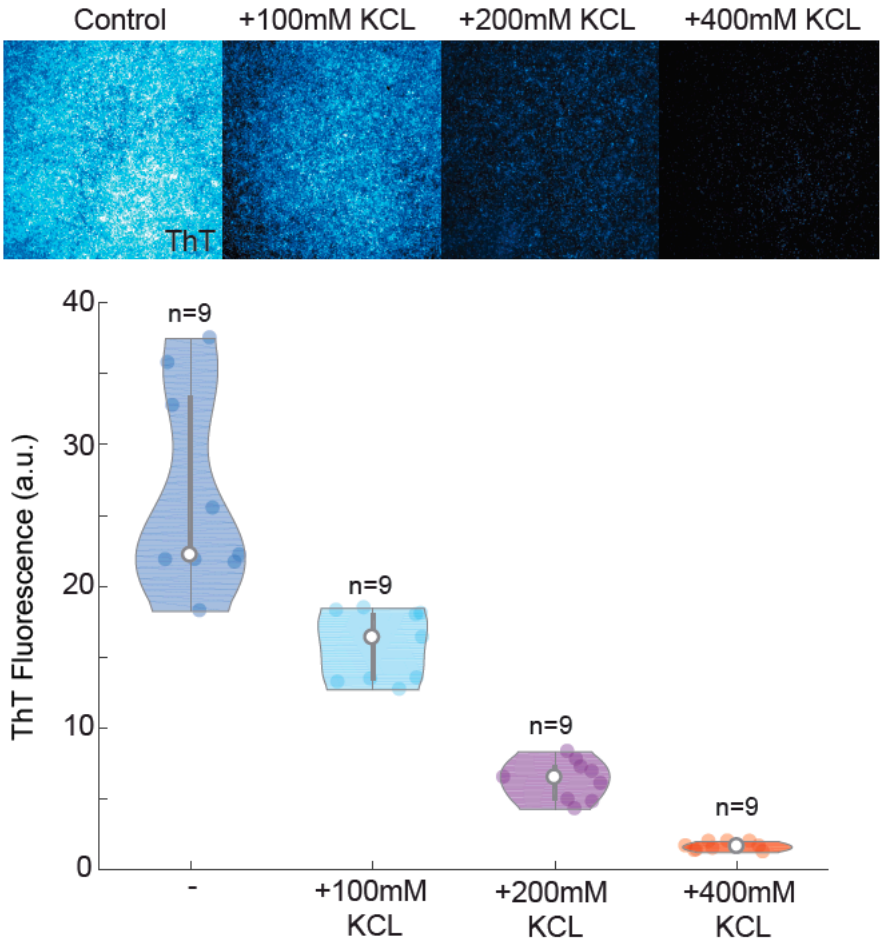

Extended Data Fig. 7. Testing ThT reporter activity in yeast cells through potassium clamp experiments.

Upper panel, screenshots from microscopy imaging of yeast after 24h in different KCL concentrations, and quantification of mean ThT fluorescence (lower panel) in independent biological replicates (n=9). Note, a near-linear drop in THT fluorescence after excessive amounts of potassium have been applied.

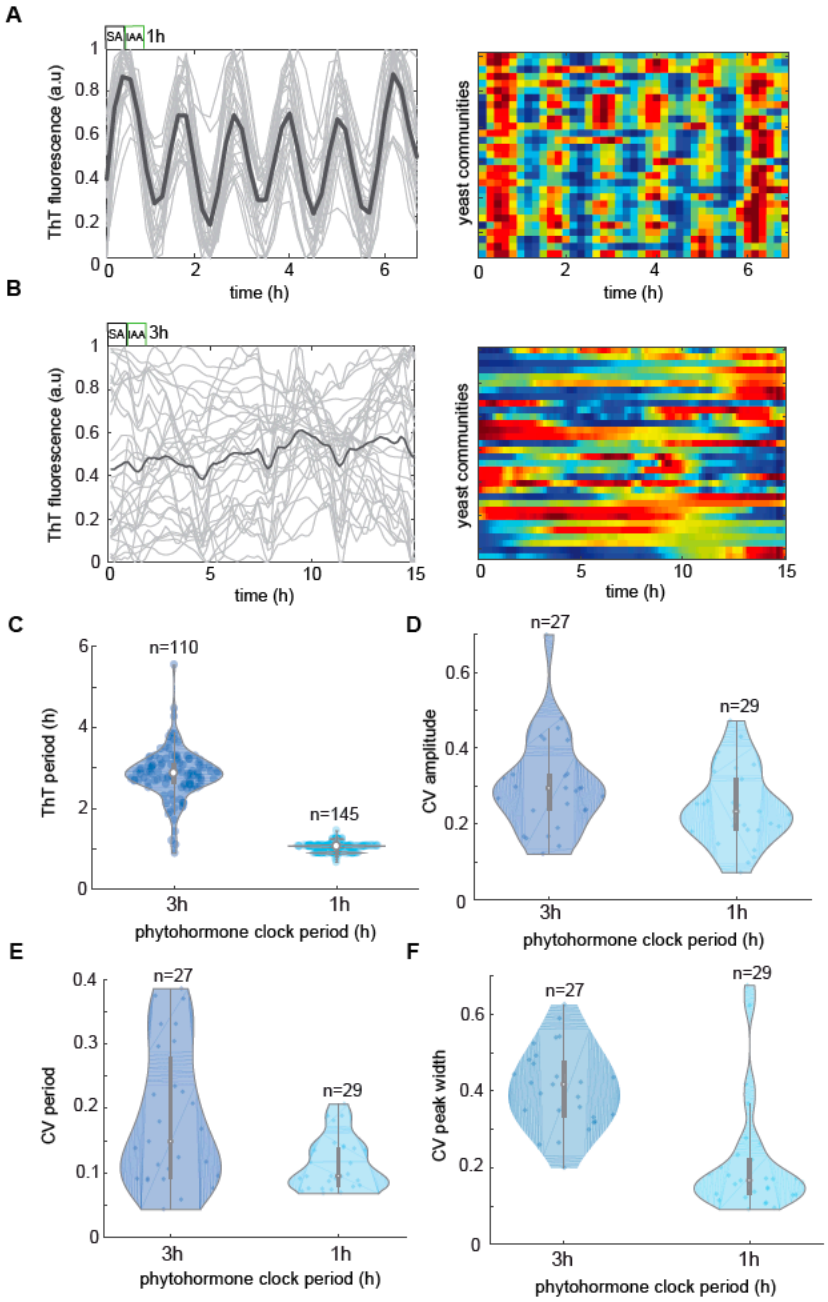

Extended Data Fig. 8. PMP firings are consistent with the environmental period of phytohormone stimuli only in the cells with the excitable circuit.

(A) Left panel, ThT fluorescence time evolutions from all traps recorded in the microfluidic device. Right panel, the heat map of ThT fluorescence for each of the recorded trapping regions corresponds to time traces (left panel) for 1-hour stimulation with antithetic IAA and SA pulses. (**B**) ThT dynamics under the 3-hour environmental stimulus (left, time course and right, heat map) in the control strain populations that lack the excitable circuit**.** Color coding as in Fig. 1**. (C)** Observed the ThT signal period in the function of the phytohormone stimulation period. **(D-F)** Coefficients of variation (CV) in the amplitude(D), periods(E), and response peak width(D) of dEGFP fluorescent reporter under different environments and stimulus periods. Note generally very low CV (CV < 1) indicates low variation in general response characteristics.

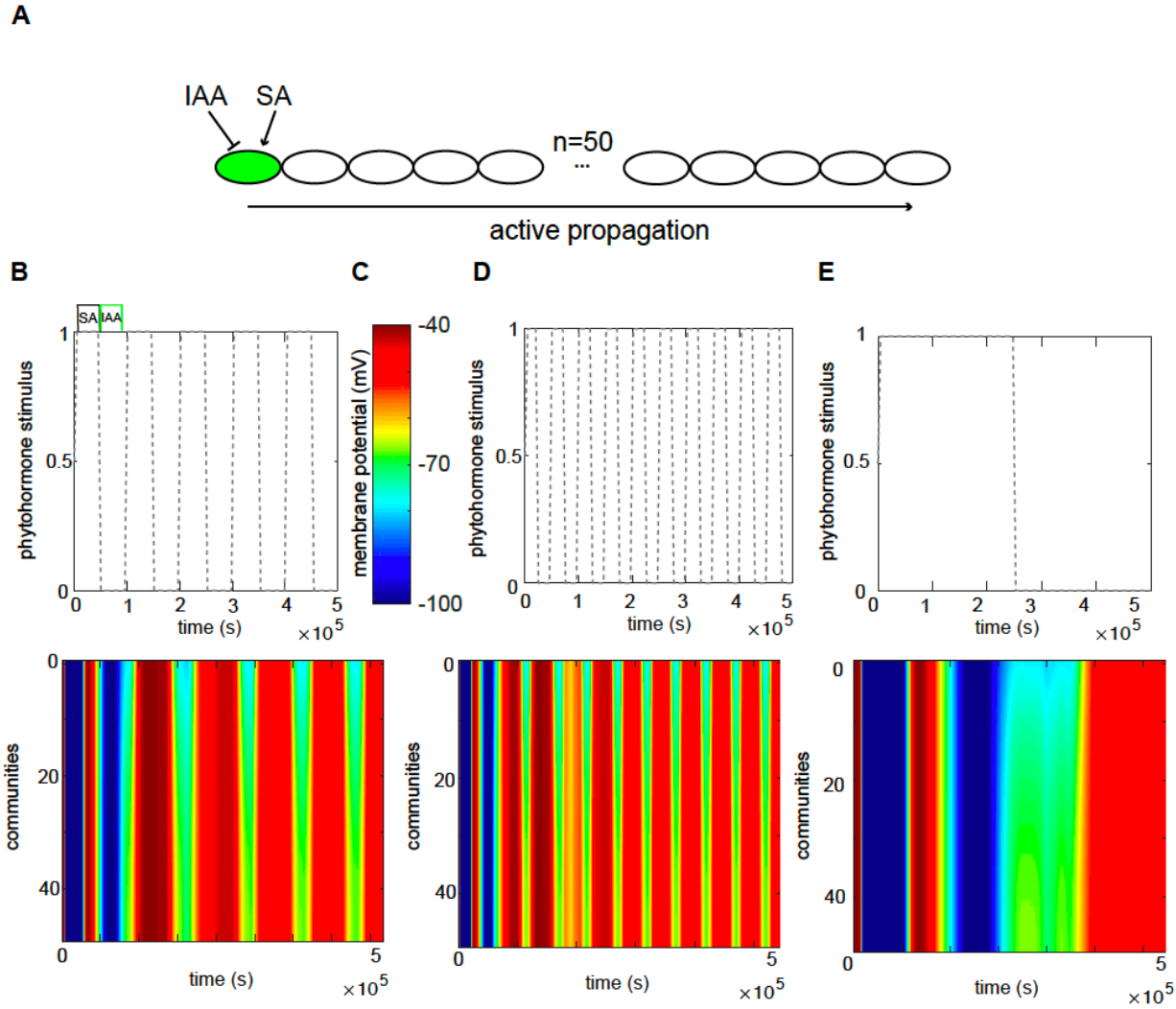

Extended Data Fig. 9. A spatial-temporal computer model predicts the active electrical signal propagation dictated by dynamic changes in ion channel abundance with the environmental pulse.

(A) Schematics of model simulation setup. The model included the 50 adjacent populations of yeast colonies. The leftmost colony is stimulated with high amplitude pulses of IAA and SA that could trigger active signal propagation by PMP changes. (**B-E**) Phytohormone stimulus function (upper panel) and predicted PMP changes (heat map, lower panel) across populations for intermediate (B), fast (D), and slow (E) phytohormone changes in the environment. (C) color coding for heat maps.

Supplementary Information

Macroscopic chemical to electrical signal converter in microbial communities

M. García-Navarrete, Merisa Avdovic, S. Pérez García, D. Ruiz Sanchis, K. Wabnik
Correspondence to: k.wabnik@upm.es

Content:

Supplementary Tables 1 and 2
Captions for Supplementary Movies 1 to 5
Captions for Data S1
Supplementary Movies 1 to 5
Data S1 [oligo and DNA sequences used in this study]

Supplementary Table 1. Model parameters.

Model parameter	Value
a_1	0.15
a_2	0.05
b_1	7.5
b_2	10
K_A	5000
K_B	75000
d_1	0.0000386(Extended Data Figs. 1A, D and 9); 0.000386(Extended Data Fig. 1B and C)
d_2	0.0000386(Extended Data Figs. 1A, B and D and 9); 0.0000965 (Extended Data Fig. 1C)
ϵ_I	0 (Extended Data Fig. 1A-C); otherwise, 10
ϵ_M	0 (Extended Data Fig. 1A-C); otherwise, 20
g_k	36
g_L	0.1
P_k	-120
P_L	-40
g_k	36
ϕ	30
a_3	0.1
d_3	40

Supplementary Table 2. Yeast strains.

Strain name	Parental strain	Composition	Markers/autotrophy
sRedM	BY4741 MATa his3Δ1 leu2Δ0 met15Δ0 ura3Δ0	BY4741 pGK1:: mCherry	KanMX (G418)
sEXGFP	sRedM	sRedM pMarIac:: IacR-VP64 (pEX1001) pMarIac::MarR-VP64 (pEX1002) pMarIac::dEGFP(pEX1003)	KanMX (G418) Leu, Ura , His
sPMPEX	BY4741 MATa his3Δ1 leu2Δ0 met15Δ0 ura3Δ0	BY4741 pMarIac:: IacR-VP64 (pEX1001) pMarIac::MarR-VP64 (pEX1002) pMarIac::KcsA* (pEX1004)	Leu, Ura , His
sEmpty(control/ sensitive strain)	BY4741 MATa his3Δ1 leu2Δ0 met15Δ0 ura3Δ0	Empty plasmids	Leu, Ura , His
sKiller	sRedM	sRedM pMarIac:: IacR-VP64 (pEX1001) pMarIac::MarR-VP64 (pEX1002) pMarIac::K1 (pEX1005)	KanMX (G418) Leu, Ura , His

Data S1. (separate file)

Oligos and synthetic DNA sequences used in this study.

Supplementary Movie 1.

Excitable gene circuit shows coordinated oscillations. Related to Fig 1.

Left Panel, Differential interference contrast (DIC), middle panel, dEGFP(cyan) and mCherry(cell marker), and right panel, dEGFP color coded in heat map colors (blue(low signal), red(high signal)) of the sampled yeast colony grow in microfluidics device with 2-hour cycles of phytohormone stimuli.

Supplementary Movie 2.

PMP oscillations controlled by phytohormone rhythms (3h stimuli). Related to Fig 2.

Left Panel, Differential interference contrast (DIC), middle panel, THT(cyan) and), and right panel, ThT color coded in heat map colors (blue(low signal), red(high signal)) of the sampled yeast colony grow in microfluidics device with 3-hour cycles of phytohormone stimuli.

Supplementary Movie 3.

PMP oscillations controlled by phytohormone rhythms (1h stimuli) (. Related to Fig 2.

Left Panel, Differential interference contrast (DIC), middle panel, THT(cyan) and), and right panel, ThT color coded in heat map colors (blue(low signal), red(high signal)) of the sampled yeast colony grow in microfluidics device with 1-hour cycles of phytohormone stimuli.

Supplementary Movie 4.

The absence of PMP oscillations in the control strain. Related to Extended Data Fig. 8B.

Left Panel, Differential interference contrast (DIC), middle panel, THT(cyan) and), and right panel, ThT color coded in heat map colors (blue(low signal), red(high signal)) of the sampled yeast colony grow in microfluidics device with 3-hour cycles of phytohormone stimuli.

Supplementary Movie 5.

PMP oscillations in sensitive strain controlled by phytohormone rhythms in cocultures. Related to Fig. 3.

Left Panel, Differential interference contrast (DIC), right panel, THT in sensitive strain (cyan) and (killer strain, mCherry of the sampled yeast two strain cocultures grow in microfluidics device with 3-hour cycles of phytohormone stimuli.